THE JOURNAL OF PHYSICAL CHEMISTRY Letters

pubs.acs.org/JPCL

Letter

Machine-Intelligence-Driven High-Throughput Prediction of 2D Charge Density Wave Phases

Arnab Kabiraj and Santanu Mahapatra*

Cite This: *J. Phys. Chem. Lett.* 2020, 11, 6291−6298

Read Online

ACCESS | Metrics & More | Article Recommendations | Supporting Information

ABSTRACT: Charge density wave (CDW) materials are an important subclass of two-dimensional materials exhibiting significant resistivity switching with the application of external energy. However, the scarcity of such materials impedes their practical applications in nanoelectronics. Here we combine a first-principles-based structure-searching technique and unsupervised machine learning to develop a fully automated high-throughput computational framework, which identifies CDW phases from a unit cell with inherited Kohn anomaly. The proposed methodology not only rediscovers the known CDW phases but also predicts a host of easily exfoliable CDW materials (30 materials and 114 phases) along with associated electronic structures. Among many promising candidates, we pay special attention to $ZrTiSe_4$ and conduct a comprehensive analysis to gain insight into the Fermi surface nesting, which causes significant semiconducting gap opening in its CDW phase. Our findings could provide useful guidelines for experimentalists.

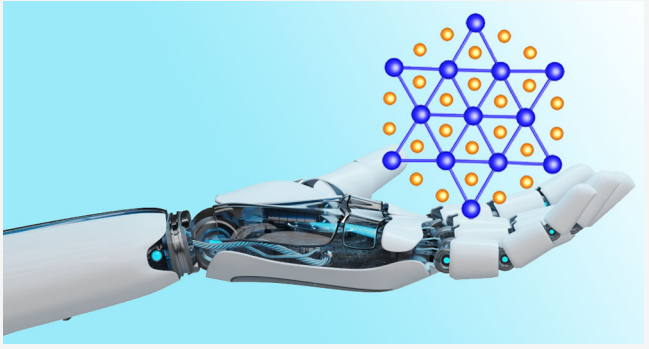

Charge density wave (CDW) is defined by a standing wave-like modulation of conduction electrons in metallic materials. The phenomenon usually arises because of instability at the Fermi surface, which stabilizes through a signature periodic lattice distortion to minimize the energy of the system.[1] Peierls showed in 1930 that for a hypothetical 1D metallic chain of atoms this kind of Fermi-level induced instability leads to an energy-gap opening at the Brillouin zone (BZ) boundary, breaking the periodicity of the lattice and generating a new unit cell with two atoms.[2] It has also been established that the energy cost to overcome the Coulomb repulsion in the lattice by this process would be countered by the band gap opening. This occurs because of the Fermi surface nesting (FSN) phenomenon, where different planes (or points in the 1D example) of the Fermi surface can be connected by a single wave vector in the BZ. Subsequently, the Peierls model also indicates that the metallic state can be stable only at high temperatures, and the material transits to the semiconducting CDW ground state below a critical temperature T_{CDW}. At the same time, Kohn demonstrated that this Fermi surface-based instability can be mapped to the vibrational (phonon) spectrum, where at the nesting vector the metallic phase must show at least one sharp dip, which is termed the Kohn anomaly, with large imaginary frequencies in its acoustic phonon branch.[3] However, just above T_{CDW}, the imaginary frequencies must disappear for the same phase, but the sharp dip in that specific branch remains, indicating the metallic phase might stabilize at temperatures above the critical temperature. For temperatures much greater than T_{CDW}, even the Kohn anomaly might fade out completely.[4] Experimental evidence of CDW was also first observed in 1D systems, though later 2D and even 3D systems with quasi-1D Fermi surface were demonstrated to show CDW.[5] On the other hand, the CDW phenomenon in some quasi-2D materials like $NbSe_2$ and TaS_2 cannot be explained with FSN alone, and the CDW in these materials has mostly been attributed to strong electron−phonon coupling.[6,7]

While the jury might still be out on the origin of CDW, the phenomenon has attracted immense attention in the nanoelectronics community owing to its lucrative electrical resistance switching associated with the metal-to-semiconductor phase change. This resistive switching in 1T-TaS_2-based systems has been achieved with the application of in-plane electric field and current[8,9] and even with optical excitations.[10] This has led to the engineering of novel CDW-based electronic devices like oscillator[11] and memristor,[9,12] while the design of more complex machinery like a transistor-less logic circuit[13] and an oscillatory neural network[14] have also been proposed.

On the other end of the spectrum, the easy mechanical exfoliation of monolayer graphene from its bulk counterpart

Received: June 14, 2020
Accepted: July 15, 2020

https://dx.doi.org/10.1021/acs.jpclett.0c01846
J. Phys. Chem. Lett. 2020, 11, 6291−6298

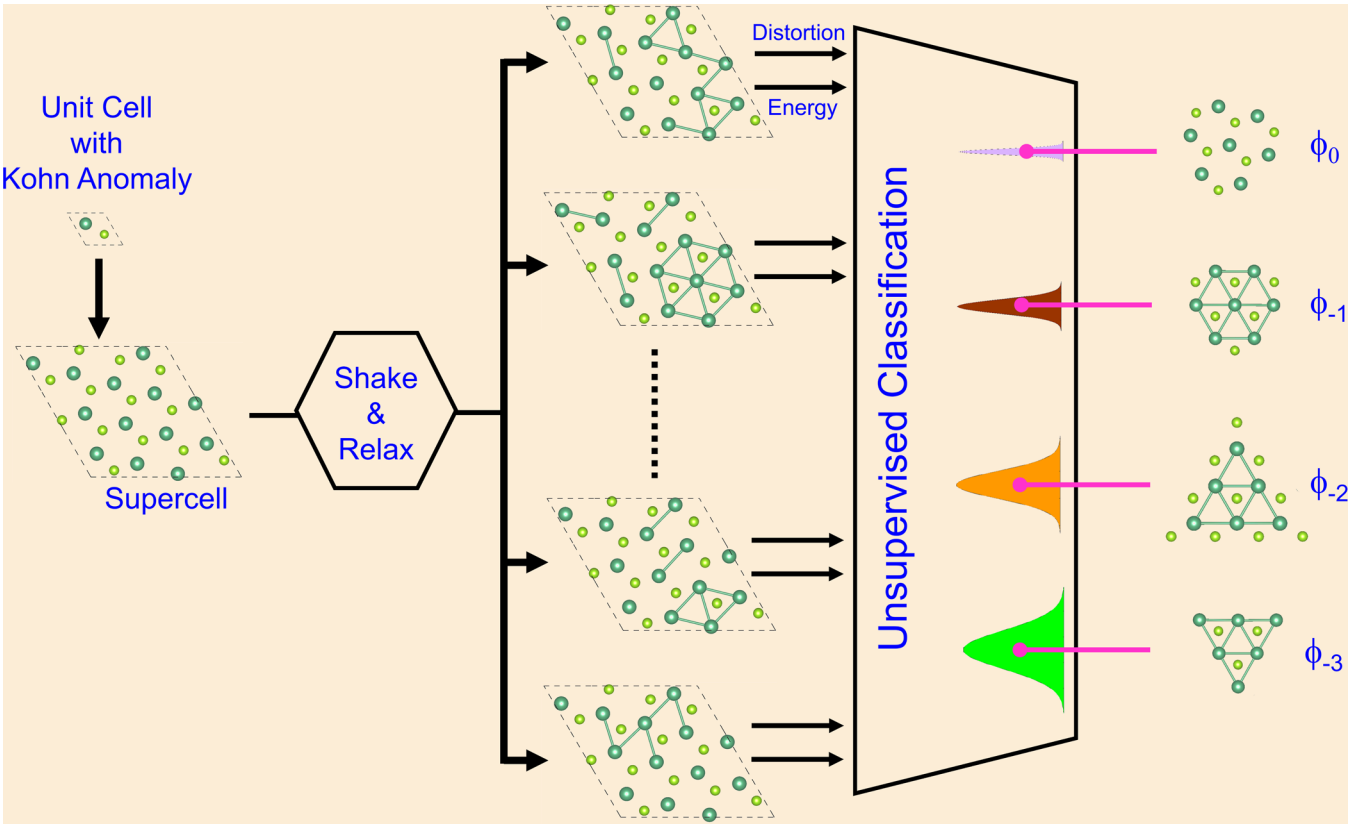

Figure 1. Automated workflow to find CDW phases of a material. A specific naming convention has been used throughout this Letter to identify the normal and CDW phases properly. The normal phase is called ϕ_0; the CDW phase just less stable than ϕ_0 is called ϕ_{-1}; the phase just less stable than ϕ_{-1} is named ϕ_{-2}, and so on.

has begun the revolutionary field of atomically thin 2D materials,[15] and a plethora of them have been discovered since by various means of exfoliation.[16] By far the most widely studied CDW materials are 1T-TaS_2 and 2H-$NbSe_2$, both being van der Walls layered materials that can be exfoliated down to the monolayer limit relatively easily.[9,17] This is also true for some other transition-metal dichalcogenide (TMD) materials exhibiting CDW, like 1T-$TaSe_2$[18] and 1T-$TiSe_2$.[19] This led to a flurry of design, implementation, and analysis of novel 2D or quasi-2D CDW-based beyond-room-temperature devices besides the previously mentioned reports, such as the study of electrical bias and temperature dependence of CDW sliding and noise,[20,21] design of all-metal proton-irradiation-immune electronics circuitry,[22] and demonstration of high-frequency current oscillation[23] which closely resembles but is fundamentally different from "narrow band noise", in quasi-2D 1T-TaS_2-based devices.

It is worth noting that in comparison with the Peierls 1D model, these real-life 2D materials exhibiting CDW show a fundamental deviation: even in the CDW phases, the band gap does not always open. However, the number of bands crossing the Fermi level, i.e. the number of states at the Fermi-level does reduce, resulting in a lower conductivity than the high-temperature normal phase.[18,24,25] Another interesting feature of these materials is the coexistence and competition of several energetically closely situated CDW phases.[8,25,26] Even the presence of thermally inaccessible "hidden" or "metastable" states in TaS_2 has been demonstrated, which can be invoked using only electrical or optical excitations.[9,10] Thus, the extensive knowledge of the stable and metastable CDW phases of a material is not only extremely important from a fundamental viewpoint but also essential for designing CDW-based devices. *Ab initio* calculations can be extremely helpful in this regard, as they are known for their excellent predictive power. However, in the case of CDW, theoretical studies seem to be driven by previous experimental observations, where the first-principles-based calculations are used as more of an analysis tool than a predictive tool.[24,25,27−29] In this work, we combine high-throughput density functional theory (DFT)-based structure-searching and unsupervised machine learning techniques to scan a host of easily exfoliable 2D materials and to predict their CDW phases with electronic properties. This extensive search unveiled a host of "new" 2D CDW materials not studied yet, some of them showing promising electronic properties that could prove to be useful for device applications.

First-principles-based high-throughput computational screening studies in 2D materials for exotic properties like nontrivial topological order,[30] high-temperature ferromagnetism,[31] or excellent catalytic activity[32] are increasingly becoming popular for materials discovery. However, developing a similar approach for CDW materials discovery is more challenging because the computation involves large supercells and the geometry optimization criteria cannot be relaxed because the energy differences between the phases are generally tiny. We adopt hardware-accelerators-based computation to overcome this challenge (see Computational Methods in the Supporting Information for details).

Recently, high-throughput computational exfoliation has been used to build a material database containing more than

https://dx.doi.org/10.1021/acs.jpclett.0c01846
J. Phys. Chem. Lett. 2020, 11, 6291−6298

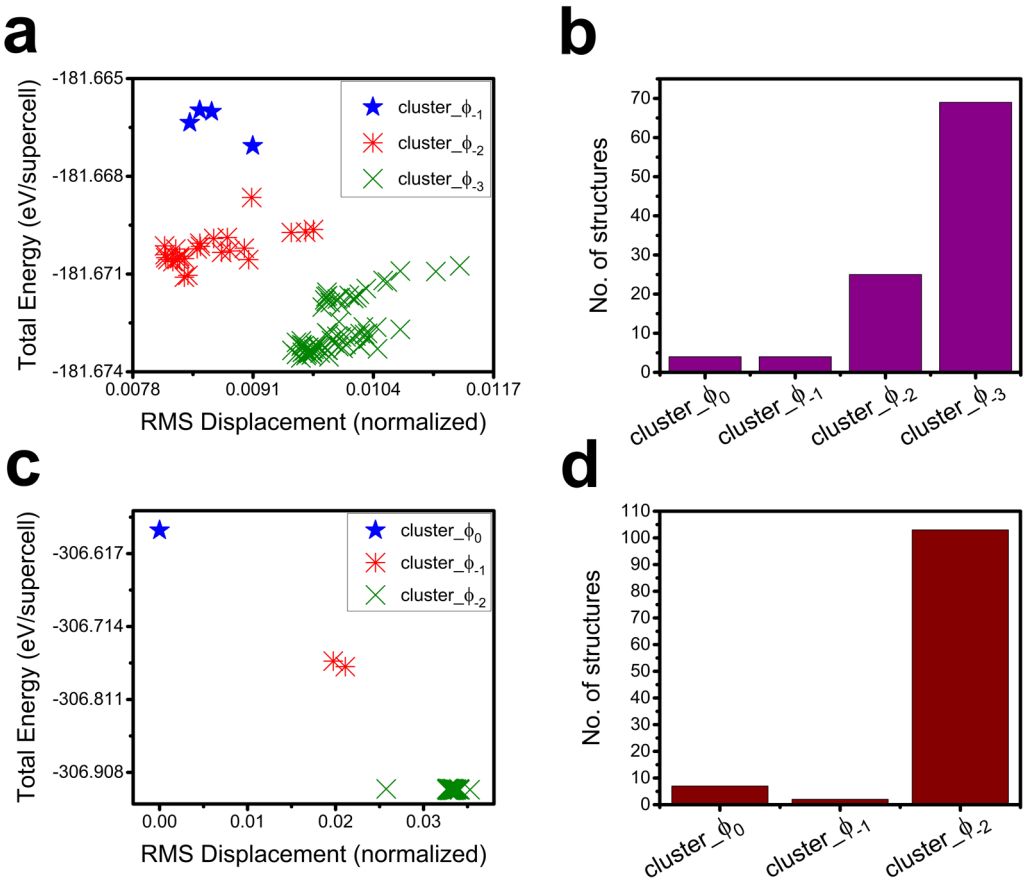

Figure 2. Unsupervised clustering of phases in the energy-distortion space. (a) Clustering of 3 × 3 $NbSe_2$ phases. Note that, in this figure, the ϕ_0 cluster is far out and could not be included in the plot. (b) Distribution of phases for 3 × 3 $NbSe_2$. (c) Clustering of $\sqrt{13} \times \sqrt{13}$ TaS_2 phases. Six points for cluster_ϕ_0 have superpositioned at the same point. (d) Distribution of phases for $\sqrt{13} \times \sqrt{13}$ TaS_2.

200 "easily exfoliable" 2D materials based on known experimental bulk structures[33] with detailed band structures and phonon spectra. From this database, we select materials with potential CDW by inspecting their metallicity and large Kohn anomaly in the phonon spectrum. We look only for nonmagnetic materials because the determination of the ground-state spin configuration for magnetic materials[31] and fine-calculation of coexistence or competition between the magnetic and CDW order is extremely challenging and beyond the scope of a high-throughput study. Apart from these, we also examine both 2H and 1T phases of all dichalcogenides (S, Se, and Te) of Ta and Nb, which are all commercially available. We further exclude the materials in the group 1T-MX_2, where M = Mo, W, and Re and X = S, Se, and Te, because it is well-known that these materials stabilize in distorted 1T (1T′ or 1T″) phases, which are still technically CDW phases, albeit with quite a large energy difference with the normal metallic phase.[34,35] Finally, we identify 35 nonmagnetic materials with potential nontrivial CDW behavior. All these materials go through our rigorous computational machinery to find the CDW phases in various supercell periodicities. However, 5 materials ($HfTe_2$, $NaPdH_2$, TiNI, YGaI, and Zr_2PTe_2) among these did not show any CDW phases in any supercells even after going through rigorous examinations. Admittedly, the acoustic phonon branches in these materials show mild to moderate imaginary frequencies, and applying the term "Kohn anomaly" might be a stretch. However, for completeness, these materials too were included in our test set. The rest of the (30) materials were all found to exhibit prominent CDW behavior.

The details of the CDW-phase-finding workflow for a material are illustrated in Figure 1. First, the unit cell of the identified material with metallic nature and Kohn anomaly is multiplied to form various supercells. To balance between computational budget and rigor, we take 2 × 2, 3 × 3, $\sqrt{13} \times \sqrt{13}$, and 4 × 4 cells for hexagonal lattices and 2 × 2, 3 × 3, and 4 × 4 cells for rectangular lattices. Note that all nontrivial reported CDW phases are covered in these periodicities; for instance, the 4 × 4 supercell covers the 4 × 1 periodicities as well.[28] These supercells are then sent through a process called "Shake & Relax", where an algorithm displaces each atom in each structure with a random direction and magnitude in the range $0 \leq d \leq a$, where d is the amount of displacement and a is a carefully chosen parameter.[36] These distorted structures are then relaxed to their nearest energy minima using rigorous DFT calculations. For each supercell, about 100 such structures are explored to sample the energy landscape reasonably. Two important aspects should be noted here: (1) The value of the parameter a is crucial to get a good sampling of the potential energy surface (PES). Too small values of a would return the structure to its initial normal state after the DFT relaxations, while too large values would push the structure away from the desired CDW energy minima and convergence problems or highly distorted structures would prevail. Our extensive test calculations reveal that the ideal "one-size-fits-all" value of a should be around 0.16 Å. Indeed,

https://dx.doi.org/10.1021/acs.jpclett.0c01846
J. Phys. Chem. Lett. 2020, 11, 6291−6298

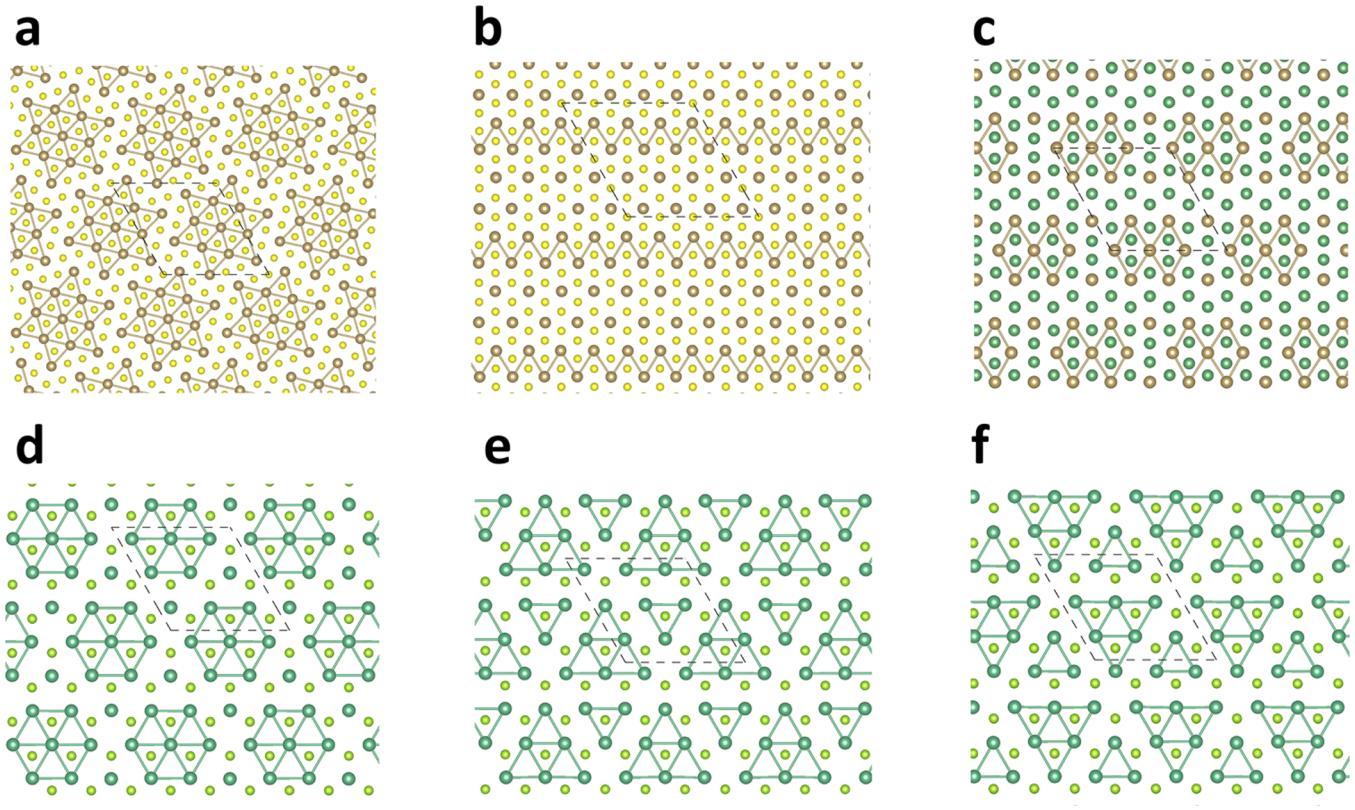

Figure 3. Reproduced CDW phases from the literature using our methodology. (a) The most stable CDW phase of 1T-TaS_2, $\sqrt{13} \times \sqrt{13}$ (ϕ_{-2}) commensurate CDW (CCDW), which is also famously called "The Star of David". The brown and yellow balls represent the Ta and S atoms, respectively. (b) Another less stable CDW phase of 1T-TaS_2, 4×4 ϕ_{-1}. (c) The most stable CDW phase of 1T-$TaTe_2$, 3×3 ϕ_{-1}. The olive balls represent the Te atoms. The 3×3 CDW phases of 2H-$NbSe_2$, (a) ϕ_{-1}, (b) ϕ_{-2} and (c) ϕ_{-3}. The dark and light green balls represent the Nb and Se atoms, respectively. For all figures, the dashed line represents the supercell boundary and the bonds are drawn only for the metal atoms coming significantly closer than the normal phase.

using this optimized value of *a*, we were able to find CDW phases for an extensive set of 2D materials. (2) Unlike other structure searching problems,[37] the geometry optimization criteria cannot be relaxed here as the difference of energy between the various CDW and normal phases can be in the order of millielectronvolt per formula-unit. At the same time, to get a good sampling of the PES, the number of explored structures cannot also be reduced significantly. This makes the computational cost of this structure-searching problem very high (see Computational Methods in the Supporting Information).

We conduct the "Shake & Relax" process for 100 distorted structures for each supercell of a given material. Previous studies of *ab initio* CDW explorations have used manual visualization to identify CDW phases from the distorted structures. Also, these phases are usually matched with experimental observations to eliminate "junk" phases. Needless to say, this process of manual phase finding can be extremely tedious and error-prone. In our case, it is nearly impossible because we deal with an enormous number of structures. Also, there is a prime chance that the manual inspection-based discovery of CDW phases might end up discarding novel "hidden" or metastable phases. We observe that the "Shake & Relax" data for a specific supercell of a particular material has two closely related properties: (1) the amount of distortion in the supercell compared to the initial normal phase and (2) the energy of the structure. We hypothesize that in a 2D space these two variables must form certain "clusters" around the stable and metastable phases. This indeed turned out to be the case after manual inspection, and we decide to employ an unsupervised clustering algorithm to find the CDW phases automatically from the data. It is found that the most popular unsupervised learning algorithm, K-Means clustering, is unsuitable here because it requires the number of clusters as input. This corresponds to the number of CDW phases which cannot be known *a priori*. Instead, we turn to the Mean Shift algorithm[38] where the number of clusters is determined by the algorithm. It has found extensive application in computer vision and image processing[39] and requires only one parameter: quantile (relating to bandwidth, see Computational Methods in the Supporting Information). Our test calculations indicate that a quantile value of 0.3−0.45 is required to discover all CDW phases thoroughly. Finally, the Mean Shift algorithm performs an unsupervised classification on the "Shake & Relax" data and reveals specific CDW phases. The structures closest to the cluster centers are taken as the representative structure of that phase, as the structures in the extrema could overlap with other clusters in some close cases.

Figure 2 depicts the distortion versus the energy plot of the two most studied 2D CDW materials and their phases, 3×3 2H-$NbSe_2$ and $\sqrt{13} \times \sqrt{13}$ 1T-TaS_2. It also delineates the distribution of structures for each cluster, which are the outcomes of the "Shake & Relax" process. While the CDW and normal phases of $\sqrt{13} \times \sqrt{13}$ 1T-TaS_2 are quite far apart in the distortion−energy plot, the 3 CDW phases of 3×3 2H-

https://dx.doi.org/10.1021/acs.jpclett.0c01846
J. Phys. Chem. Lett. 2020, 11, 6291−6298

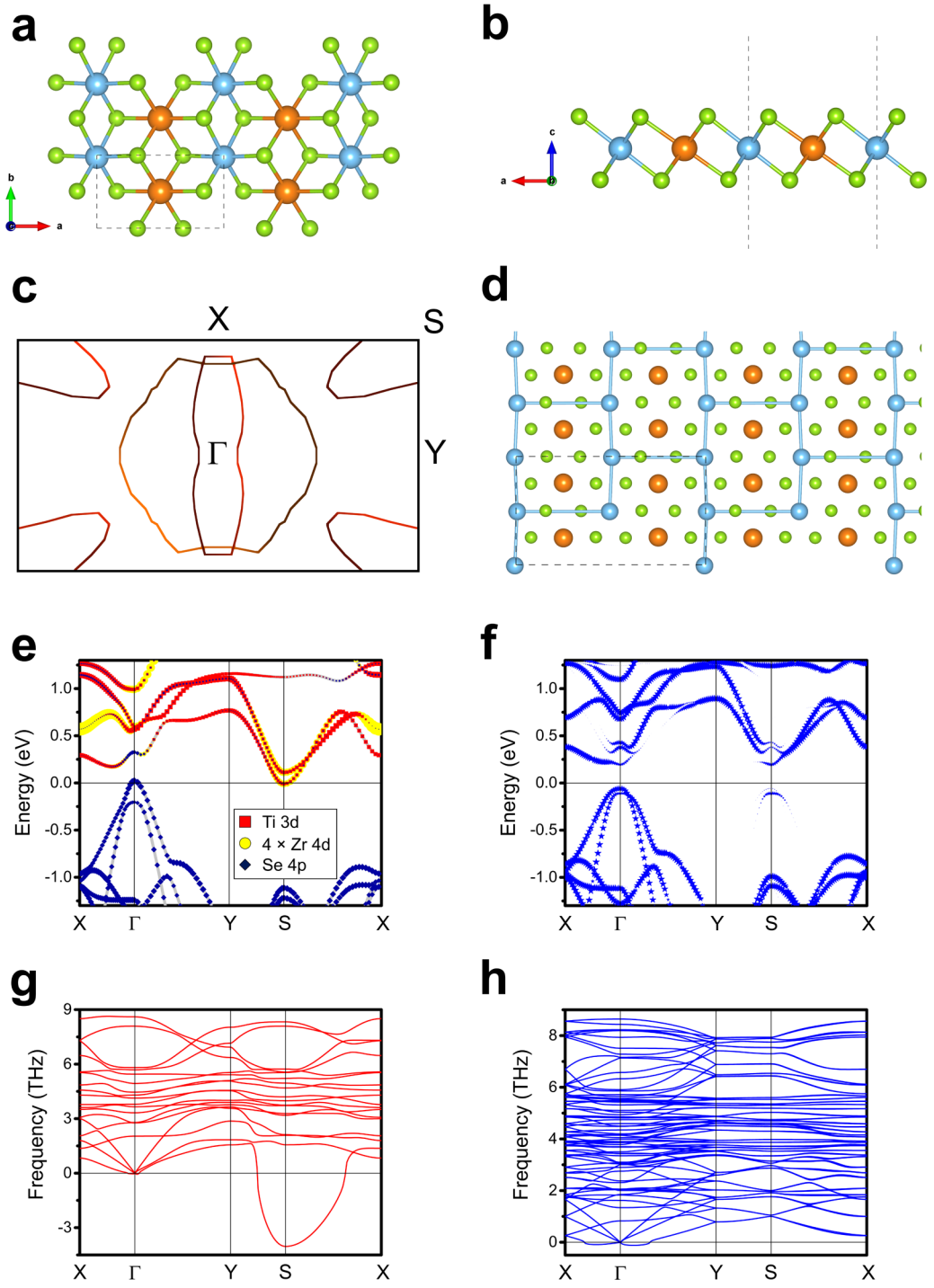

Figure 4. Details of $ZrTiSe_4$. (a) Top and (b) side view of the $ZrTiSe_4$ crystal structure. The orange, blue, and green balls represent the Zr, Ti, and Se atoms, respectively. The dashed line indicates the boundary of the unit cell. (c) Fermi surface along with the Brillouin zone of $ZrTiSe_4$. (d) Most stable CDW phase, 2×2 ϕ_{-1} of the material. Horizontal Ti−Ti distances are 6.49 and 6.2 Å here. The blue lines are drawn for Ti−Ti distance <6.36 Å, which is the distance in the normal phase. The dashed line indicates the 2×2 cell boundary. (e) Total and elemental orbital resolved band structure of $ZrTiSe_4$. The size of the symbols defines the weight of a particular orbital, and the Fermi level has been set as zero energy. Note that the contribution of Zr 4d is magnified 4 times for visualization purposes. (f) Unfolded band structure of the 2×2 ϕ_{-1} CDW phase. The size of the symbols represents the weight at a particular k-location. (g) Phonon dispersion of the normal phase of the material. The imaginary frequencies have been represented as negative frequencies. (h) Phonon dispersion of the 2×2 ϕ_{-1} CDW phase. Mind the effect of BZ folding here.

$NbSe_2$ are quite closely situated and can be difficult to identify without the clustering algorithm.

Figure 3 shows the CDW phases found by our methodology for 1T-TaS_2, $TaSe_2$, and 2H-$NbSe_2$, which almost exactly reproduce phases as well as energies reported in the literature.[27,28] Note that the "hidden" 3×3 hexagonal phase of $NbSe_2$[27] (Figure 3d) has been missed by many studies probably because the experimental demonstration of this phase is scarce.[24,25]

https://dx.doi.org/10.1021/acs.jpclett.0c01846
J. Phys. Chem. Lett. 2020, 11, 6291−6298

Table S1 tabulates all the proper CDW phases we have found through our search, their energy differences with the normal phase, and their band gap or ($\sqrt{13} \times \sqrt{13}$ 1T-TaS_2-like) CDW-gap,[29] i.e., the energy-difference between the highest point of the band right below and the lowest point of the band immediately above the Fermi level. Images of crystal structures, as well as band structures of interesting CDW materials, are also included in the Supporting Information. While analyzing the data, we make some important observations, which are summarized below.

A total of 3 materials show CDW-gap like the $\sqrt{13} \times \sqrt{13}$ 1T-TaS_2 phase. $\sqrt{13} \times \sqrt{13}$ 1T-NbS_2 and $\sqrt{13} \times \sqrt{13}$ 1T-$TaSe_2$, both manifesting "Star of David" patterns, show a CDW-gap close to that of the $\sqrt{13} \times \sqrt{13}$ 1T-TaS_2 phase, while the energy difference between the CDW phase and the normal phase is much greater in the latter case compared to TaS_2. The $\sqrt{13} \times \sqrt{13}$ 2H-$NbTe_2$ CDW phases show smaller CDW-gaps with much smaller energy differences. More interestingly, six materials found by our search exhibits significant band gap opening in their CDW phases. Among these, the most stable 2 × 2 CDW phases of 1T-$TiCl_2$ and $TiBr_2$ exhibit transition from 1T to 1T′ phase like MoS_2[34] but show unique CDW patterns in larger supercells. Although the band gap opening is significant here, the energy difference with the 1T phase is also extremely high. The predicted CDW phase and the band gap opening of TiS_2 (1T) are in good agreement with a previous report.[40] The 2 × 2 VOCl ϕ_{-2} phase also shows a moderate band gap with a relatively sizable energy difference.

We observe that 1T-NbS_2 exhibits almost identical CDW phases as 1T-TaS_2, both in terms of geometry or bond-lengths and energetics. While almost all room-temperature CDW devices to date have been built using 1T-TaS_2 with the properties being extensively studied, 1T-NbS_2 has been somewhat ignored, perhaps because of the naturally superior stability of the 2H phase. However, our calculations hint that 1T-NbS_2 might be a suitable alternative for 1T-TaS_2. In fact, all the dichalcogenides of Ta and Nb show many similar CDW patterns.

Even for the extensively studied materials, our search finds some previously undiscovered phases, such as the 2 × 2 phases of 2H-$NbSe_2$[27] and the 3 × 3 CDW of 1T-TaS_2,[28] although all of them are energetically inferior to other phases. It is worth mentioning that we do get a few phases with no apparent symmetry, especially in larger periodicities. These could be "junk" phases resulting from a loss of BZ sampling for larger cells, but most probably are caused by local minima pockets in the PES as we do find these in clusters of 2−10 structures. These phases could very well be "hidden" or metastable phases.

Among many promising candidates, we pay special attention to $ZrTiSe_4$. For this material, the most stable CDW phase is the 2 × 2 CDW, where a decent band gap opening (0.25 eV) and a moderate energy difference with the normal phase (4 meV/formula-unit) is observed. In 3 × 3 periodicity, the material shows much weaker (0.14 and 0.58 meV/formula-unit) metallic CDWs, bringing in a varying amount of resistivity. Figure 4 illustrates the minute details of the material and its 2 × 2 CDW. $ZrTiSe_4$ inherits a rectangular lattice. The Fermi surface of the normal metallic phase is visualized in Figure 4c. The round-shaped surface around the Γ point originates from the band coming from below the Fermi level, whereas the elongated surfaces around the Γ point and at the S point originate from the band situated mostly above the Fermi level. The quasi-1D nature of the Fermi surface near the S point hints that the CDW in this material most probably originates from FSN. Figure 4e shows the electronic band structure, and Figure 4g shows the phonon dispersion of the normal phase. The phonon dispersion shows a giant Kohn anomaly with imaginary frequencies at and around the S point, and the electronic band structure shows two bands crossing the Fermi level, one coming from below at Γ and another coming from above at the S point. Despite using different DFT codes, these results are in agreement with the previous report.[33] In the 2 × 2 CDW (Figure 4d), the Ti atom situated at the S point gets modulated slightly, which creates a ladder-like network of Ti atoms: two horizontal (along vector **b**) Ti ions coming closer, while the next two are moving away from each other. This opens a significant band gap in the CDW phase (Figure 4f) while the Kohn anomaly along with its imaginary frequencies vanishes (Figure 4h) and establishes a stable phase at low temperatures.

The proposed methodology, though rigorous, is limited by computational budget, and hence, the search for CDWs in a supercell beyond 4 × 4 becomes quite difficult. Also, the mandatory loss of *k*-points sampling in these larger supercells might reduce the accuracy of the prediction. However, in real life, many important CDW phases might occur in larger periodicities, such as the low-resistance noncommensurate (NC) CDW phase of 1T-TaS_2 which is frequently exploited in 2D CDW devices.[9,11] Phases such as these are still beyond the reach of first-principles-based calculations.

Although here we explore only monolayered materials for possible CDW phases, in reality, exfoliation down to the monolayer is difficult, and many samples that show CDW phases in experiments contain at least a few layers. Our computational methodology should work seamlessly for few-layered materials as well, although the computational cost would become exponentially higher with the addition of more layers. Besides this, the van der Walls interaction between the layers must be considered while performing the high-throughput DFT calculations which might increase the computational expense further.

To summarize, in this work we have developed an automated, machine-intelligence-driven, true first-principles-based methodology to find the CDW phases of any 2D material. The method is rigorous and mostly free of manual errors and is capable of finding even subtle "hidden" or "metastable" CDW phases. Using this methodology, we search a computationally exfoliated 2D materials database to find quite a few CDW phases with CDW-gap as well as true band gap with various amounts of energy differences with the normal phase. Many of these materials have already been synthesized and are likely to be synthesized in the future, giving engineers a variety of options to choose from according to their device requirements. We also provide theoretical insights on a promising CDW material, $ZrTiSe_4$, in which a significant band gap opening occurs, which in turn should exhibit a metal-to-insulator transition. However, the energy required to achieve such a transition is only about 1/6th of that required for 1T-TaS_2 resistive switching. Our work might foster theoretical insights into different 2D CDW materials and accelerate practical device applications.

https://dx.doi.org/10.1021/acs.jpclett.0c01846
J. Phys. Chem. Lett. 2020, 11, 6291−6298

■ ASSOCIATED CONTENT

Supporting Information

The Supporting Information is available free of charge at https://pubs.acs.org/doi/10.1021/acs.jpclett.0c01846.

Table of CDW phases, their energy differences with the normal phase and band/CDW-gaps, chosen images of CDW crystal structures and band structures, computational methods, and supporting references (PDF)

■ AUTHOR INFORMATION

Corresponding Author

Santanu Mahapatra − *Nano-Scale Device Research Laboratory, Department of Electronic Systems Engineering, Indian Institute of Science (IISc) Bangalore, Bangalore 560012, India;* orcid.org/0000-0003-1112-8109; Email: santanu@iisc.ac.in

Author

Arnab Kabiraj − *Nano-Scale Device Research Laboratory, Department of Electronic Systems Engineering, Indian Institute of Science (IISc) Bangalore, Bangalore 560012, India;* orcid.org/0000-0002-7063-0169

Complete contact information is available at: https://pubs.acs.org/10.1021/acs.jpclett.0c01846

Author Contributions

A.K. performed the DFT calculations, designed and implemented the computational methodology combining hybrid processor-based structure searching and unsupervised learning, and analyzed the results. S.M. conceived the problem statement and overall supervised the work. All authors contributed to the writing.

Notes

The authors declare no competing financial interest.

All CDW crystal structure files (cif) and their top-view images (png) are available at the OSF repository (https://osf.io/by7et).

■ ACKNOWLEDGMENTS

This work was supported by the Mathematical Research Impact Centric Support (MATRICS) scheme of Science and Engineering Research Board (SERB), Government of India, under grant number MTR/2019/000047. The authors thank the Supercomputer Education and Research Centre (SERC), Indian Institute of Science (IISc) Bangalore, for GPU- and Xeon-Phi-based computations.

■ REFERENCES

(1) Thorne, R. E. Charge-Density-Wave Conductors. *Phys. Today* **1996**, *49* (5), 42−47.

(2) Peierls, R. E. *Quantum Theory of Solids*; Oxford University Press, 1955.

(3) Kohn, W. Image of the Fermi Surface in the Vibration Spectrum of a Metal. *Phys. Rev. Lett.* **1959**, *2* (9), 393−394.

(4) Zhu, X.; Cao, Y.; Zhang, J.; Plummer, E. W.; Guo, J. Classification of Charge Density Waves Based on Their Nature. *Proc. Natl. Acad. Sci. U. S. A.* **2015**, *112* (8), 2367−2371.

(5) Chen, C.-W.; Choe, J.; Morosan, E. Charge Density Waves in Strongly Correlated Electron Systems. *Rep. Prog. Phys.* **2016**, *79* (8), 084505.

(6) Johannes, M. D.; Mazin, I. I.; Howells, C. A. Fermi-Surface Nesting and the Origin of the Charge-Density Wave in $NbSe_2$. *Phys. Rev. B: Condens. Matter Mater. Phys.* **2006**, *73* (20), 205102.

(7) Johannes, M. D.; Mazin, I. I. Fermi Surface Nesting and the Origin of Charge Density Waves in Metals. *Phys. Rev. B: Condens. Matter Mater. Phys.* **2008**, *77* (16), 165135.

(8) Tsen, A. W.; Hovden, R.; Wang, D.; Kim, Y. D.; Okamoto, J.; Spoth, K. A.; Liu, Y.; Lu, W.; Sun, Y.; Hone, J. C.; Kourkoutis, L. F.; Kim, P.; Pasupathy, A. N. Structure and Control of Charge Density Waves in Two-Dimensional 1T-TaS_2. *Proc. Natl. Acad. Sci. U. S. A.* **2015**, *112* (49), 15054−15059.

(9) Yoshida, M.; Suzuki, R.; Zhang, Y.; Nakano, M.; Iwasa, Y. Memristive Phase Switching in Two-Dimensional 1T-TaS_2 Crystals. *Sci. Adv.* **2015**, *1* (9), No. e1500606.

(10) Stojchevska, L.; Vaskivskyi, I.; Mertelj, T.; Kusar, P.; Svetin, D.; Brazovskii, S.; Mihailovic, D. Ultrafast Switching to a Stable Hidden Quantum State in an Electronic Crystal. *Science* **2014**, *344* (6180), 177−180.

(11) Liu, G.; Debnath, B.; Pope, T. R.; Salguero, T. T.; Lake, R. K.; Balandin, A. A. A Charge-Density-Wave Oscillator Based on an Integrated Tantalum Disulfide-Boron Nitride-Graphene Device Operating at Room Temperature. *Nat. Nanotechnol.* **2016**, *11* (10), 845−850.

(12) Sun, Y.; Dai, T.; He, Z.; Zhou, W.; Hu, P.; Li, S.; Wu, S. Memristive Phase Switching in Two-Dimensional 1T′-VSe_2 Crystals. *Appl. Phys. Lett.* **2020**, *116* (3), 033101.

(13) Khitun, A. G.; Geremew, A. K.; Balandin, A. A. Transistor-Less Logic Circuits Implemented With 2-D Charge Density Wave Devices. *IEEE Electron Device Lett.* **2018**, *39* (9), 1449−1452.

(14) Khitun, A.; Liu, G.; Balandin, A. A. Two-Dimensional Oscillatory Neural Network Based on Room-Temperature Charge-Density-Wave Devices. *IEEE Trans. Nanotechnol.* **2017**, *16* (5), 860−867.

(15) Novoselov, K. S.; Geim, A. K.; Morozov, S. V.; Jiang, D.; Zhang, Y.; Dubonos, S. V.; Grigorieva, I. V.; Firsov, A. A. Electric Field Effect in Atomically Thin Carbon Films. *Science* **2004**, *306* (5696), 666−669.

(16) Das, S.; Kim, M.; Lee, J.; Choi, W. Synthesis, Properties, and Applications of 2-D Materials: A Comprehensive Review. *Crit. Rev. Solid State Mater. Sci.* **2014**, *39* (4), 231−252.

(17) Xi, X.; Zhao, L.; Wang, Z.; Berger, H.; Forró, L.; Shan, J.; Mak, K. F. Strongly Enhanced Charge-Density-Wave Order in Monolayer $NbSe_2$. *Nat. Nanotechnol.* **2015**, *10* (9), 765−769.

(18) Ryu, H.; Chen, Y.; Kim, H.; Tsai, H.-Z.; Tang, S.; Jiang, J.; Liou, F.; Kahn, S.; Jia, C.; Omrani, A. A.; Shim, J. H.; Hussain, Z.; Shen, Z.-X.; Kim, K.; Min, B. Il; Hwang, C.; Crommie, M. F.; Mo, S.-K. Persistent Charge-Density-Wave Order in Single-Layer $TaSe_2$. *Nano Lett.* **2018**, *18* (2), 689−694.

(19) Chen, P.; Chan, Y.-H.; Fang, X.-Y.; Zhang, Y.; Chou, M. Y.; Mo, S.-K.; Hussain, Z.; Fedorov, A.-V.; Chiang, T.-C. Charge Density Wave Transition in Single-Layer Titanium Diselenide. *Nat. Commun.* **2015**, *6* (1), 8943.

(20) Liu, G.; Rumyantsev, S.; Bloodgood, M. A.; Salguero, T. T.; Balandin, A. A. Low-Frequency Current Fluctuations and Sliding of the Charge Density Waves in Two-Dimensional Materials. *Nano Lett.* **2018**, *18* (6), 3630−3636.

(21) Geremew, A. K.; Rumyantsev, S.; Kargar, F.; Debnath, B.; Nosek, A.; Bloodgood, M. A.; Bockrath, M.; Salguero, T. T.; Lake, R. K.; Balandin, A. A. Bias-Voltage Driven Switching of the Charge-Density-Wave and Normal Metallic Phases in 1T-TaS_2 Thin-Film Devices. *ACS Nano* **2019**, *13* (6), 7231−7240.

(22) Geremew, A. K.; Kargar, F.; Zhang, E. X.; Zhao, S. E.; Aytan, E.; Bloodgood, M. A.; Salguero, T. T.; Rumyantsev, S.; Fedoseyev, A.; Fleetwood, D. M.; Balandin, A. A. Proton-Irradiation-Immune Electronics Implemented with Two-Dimensional Charge-Density-Wave Devices. *Nanoscale* **2019**, *11* (17), 8380−8386.

(23) Geremew, A. K.; Rumyantsev, S.; Debnath, B.; Lake, R. K.; Balandin, A. A. High-Frequency Current Oscillations in Charge-Density-Wave 1T-TaS_2 Devices: Revisiting the "Narrow Band Noise" Concept. *Appl. Phys. Lett.* **2020**, *116* (16), 163101.

(24) Lian, C.-S.; Si, C.; Duan, W. Unveiling Charge-Density Wave, Superconductivity, and Their Competitive Nature in Two-Dimensional $NbSe_2$. *Nano Lett.* **2018**, *18* (5), 2924−2929.
(25) Gye, G.; Oh, E.; Yeom, H. W. Topological Landscape of Competing Charge Density Waves in 2H-$NbSe_2$. *Phys. Rev. Lett.* **2019**, *122* (1), 16403.
(26) Ugeda, M. M.; Bradley, A. J.; Zhang, Y.; Onishi, S.; Chen, Y.; Ruan, W.; Ojeda-Aristizabal, C.; Ryu, H.; Edmonds, M. T.; Tsai, H.-Z.; Riss, A.; Mo, S.-K.; Lee, D.; Zettl, A.; Hussain, Z.; Shen, Z.-X.; Crommie, M. F. Characterization of Collective Ground States in Single-Layer $NbSe_2$. *Nat. Phys.* **2016**, *12* (1), 92−97.
(27) Cossu, F.; Moghaddam, A. G.; Kim, K.; Tahini, H. A.; Di Marco, I.; Yeom, H.-W.; Akbari, A. Unveiling Hidden Charge Density Waves in Single-Layer $NbSe_2$ by Impurities. *Phys. Rev. B: Condens. Matter Mater. Phys.* **2018**, *98* (19), 195419.
(28) Miller, D. C.; Mahanti, S. D.; Duxbury, P. M. Charge Density Wave States in Tantalum Dichalcogenides. *Phys. Rev. B: Condens. Matter Mater. Phys.* **2018**, *97* (4), 045133.
(29) Yi, S.; Zhang, Z.; Cho, J. H. Coupling of Charge, Lattice, Orbital, and Spin Degrees of Freedom in Charge Density Waves in 1T- TaS_2. *Phys. Rev. B: Condens. Matter Mater. Phys.* **2018**, *97* (4), 041413.
(30) Marrazzo, A.; Gibertini, M.; Campi, D.; Mounet, N.; Marzari, N. Relative Abundance of Z2 Topological Order in Exfoliable Two-Dimensional Insulators. *Nano Lett.* **2019**, *19* (12), 8431−8440.
(31) Kabiraj, A.; Kumar, M.; Mahapatra, S. High-Throughput Discovery of High Curie Point Two-Dimensional Ferromagnetic Materials. *npj Comput. Mater.* **2020**, *6* (1), 35.
(32) Karmodak, N.; Andreussi, O. Catalytic Activity and Stability of Two-Dimensional Materials for the Hydrogen Evolution Reaction. *ACS Energy Lett.* **2020**, *5* (3), 885−891.
(33) Mounet, N.; Gibertini, M.; Schwaller, P.; Campi, D.; Merkys, A.; Marrazzo, A.; Sohier, T.; Castelli, I. E.; Cepellotti, A.; Pizzi, G.; Marzari, N. Two-Dimensional Materials from High-Throughput Computational Exfoliation of Experimentally Known Compounds. *Nat. Nanotechnol.* **2018**, *13* (3), 246−252.
(34) Zhuang, H. L.; Johannes, M. D.; Singh, A. K.; Hennig, R. G. Doping-Controlled Phase Transitions in Single-Layer MoS_2. *Phys. Rev. B: Condens. Matter Mater. Phys.* **2017**, *96* (16), 165305.
(35) Choi, J.-H.; Jhi, S.-H. Origin of Distorted 1T-Phase ReS_2: First-Principles Study. *J. Phys.: Condens. Matter* **2018**, *30* (10), 105403.
(36) Pickard, C. J; Needs, R J Ab Initio Random Structure Searching. *J. Phys.: Condens. Matter* **2011**, *23* (5), 053201.
(37) Kabiraj, A.; Mahapatra, S. Intercalation-Driven Reversible Switching of 2D Magnetism. *J. Phys. Chem. C* **2020**, *124* (1), 1146−1157.
(38) Comaniciu, D.; Meer, P. Mean Shift: A Robust Approach toward Feature Space Analysis. *IEEE Trans. Pattern Anal. Mach. Intell.* **2002**, *24* (5), 603−619.
(39) Chris, T.; Karamchandani, S.; Biradar, T. Review of Mean Shift Algorithm and Its Improvements. *IJCA Proc. Int. Conf. Comput. Technol.* **2015**, No. 5, 25−30.
(40) Dolui, K.; Sanvito, S. Dimensionality-Driven Phonon Softening and Incipient Charge Density Wave Instability in TiS2. *Epl* **2016**, *115* (4), 47001.

https://dx.doi.org/10.1021/acs.jpclett.0c01846
J. Phys. Chem. Lett. 2020, 11, 6291−6298